

Urban air quality: What is the optimal place to reduce transport emissions?

Original

Urban air quality: What is the optimal place to reduce transport emissions? / Li, T., Fellini, S., van Reeuwijk, M.. - In: ATMOSPHERIC ENVIRONMENT. - ISSN 1352-2310. - 292:(2023), p. 119432. [10.1016/j.atmosenv.2022.119432]

Availability:

This version is available at: 11583/2974159 since: 2022-12-24T11:52:49Z

Publisher:

Elsevier

Published

DOI:10.1016/j.atmosenv.2022.119432

Terms of use:

This article is made available under terms and conditions as specified in the corresponding bibliographic description in the repository

Publisher copyright

(Article begins on next page)

Urban air quality: what is the optimal place to reduce transport emissions?

Tianyang Li¹, Sofia Fellini², Maarten van Reeuwijk^{1,a}

¹ Department of Civil and Environmental Engineering, Imperial College London, SW7 2AZ London

² Univ Lyon, INSA Lyon, CNRS, Ecole Centrale de Lyon, Univ Claude Bernard Lyon 1, LMFA,
UMR5509, 69621, Villeurbanne France.

^a Email: m.vanreeuwijk@imperial.ac.uk

Abstract

We develop a linear model based on a complex network approach that predicts the effect of emission changes on air pollution exposure in urban street networks including NO-NO₂-O₃-chemistry. The operational air quality model SIRANE is used to create a weighted adjacency matrix A describing the relation between emissions of a passive scalar inside streets and the resulting concentrations in the street network. A case study in South Kensington (London) is used, and the adjacency matrix A_0 is determined one wind speed and eight different wind directions. The physics of the underlying problem is used to infer A for different wind speeds. Good agreement between SIRANE predictions and the model is observed for all but the lowest wind speed, despite non-linearities in SIRANE's model formulation. An indicator for exposure in the street is developed, and it is shown that the out-degree of the exposure matrix E represents the effect of a change in emissions on the exposure reduction in all streets in the network. The approach is then extended to NO-NO₂-O₃-chemistry, which introduces a non-linearity. It is shown that a linearised model agrees well with the fully nonlinear SIRANE predictions. The model shows that roads with large height-to-width ratios are the first in which emissions should be reduced in order to maximise exposure reduction.

25 1. Introduction

26 Almost all the global population (99%) is exposed to pollution levels that exceeds WHO limits, with
27 middle- and low-income countries hit hardest (WHO, 2021). With the progressive shift of people from
28 rural to urban areas, city administrations are urged to develop effective air quality plans to meet air
29 quality standards and protect citizens' health. These plans mainly concern the control of vehicular
30 traffic which is the most important source driving exceedances of air quality standards across city
31 centres (EEA, 2022). For traffic control policies (Lu et al., 2021; Wu et al., 2017) to be effective, it is
32 essential to quantify the contribution of local traffic emissions to the pollution levels of the urban area
33 in order to optimally identify the places to impose restrictions. Methods for quantifying source-
34 receptor relationship are known as source apportionment techniques (Wagstrom et al., 2008; Koo et
35 al., 2009; Clappier et al., 2017) and the most common are based on simulations using air quality
36 models.

37 Modelling air pollution in urban areas is far from trivial as flow and dispersion dynamics are strongly
38 influenced by the presence of buildings, their geometric properties, and the orientation of the streets.
39 Moreover, polluting emissions and exposure targets (i.e. citizens) are characterized by temporal and
40 spatial patterns that make the analysis more complex. Further modelling issues are encountered when
41 dealing with reactive pollutants. This is the case of nitrogen oxides (NO_2 , NO) which are formed in
42 combustion processes (mainly from vehicular traffic) and undergo a series of photochemical reactions
43 with the secondary formation of ozone. Acute exposure to these pollutants causes respiratory
44 diseases and paediatric asthma (Khreis et al., 2017; Anenberg et al., 2022). Since the reaction times of
45 NO_2 - NO - O_3 chemistry are comparable to their residence times in the streets (that is governed by
46 turbulent transport) these transformations must be taken into account to predict air pollution at the
47 district and street scales (Derwent & Middleton, 1996; Mchugh et al., 1997; Soulhac et al., 2011) and
48 its impact on citizen's health.

49 Computational fluid dynamic (CFD) simulations can be effectively used to model flow, dispersion, and
50 chemical reactions (Baker et al., 2004; Bright et al., 2013; Grylls et al., 2019; Zhang et al., 2020) in
51 complex geometries. However, they are computationally expensive and require a large amount of
52 detailed input data. The adoption of simplified modelling techniques is the most efficient option when
53 dealing with urban areas consisting of hundreds of streets and when the goal is to explore multiple
54 emission and exposure scenarios.

55 To this aim, street network models have been developed in the last decades (Berkowicz, 2000; Kim et
56 al., 2018; McHugh et al., 1997; Soulhac et al., 2011). These are operational tools for air quality
57 modelling based on the description of the urban fabric as a network of streets of homogeneous
58 pollutant concentration. Each street is characterized by a polluting source and by the average
59 geometric properties of the buildings. In this way, the complex urban pattern of buildings is
60 represented by a simplified and regular domain of links (the streets) and nodes (street intersections).
61 The wind flow and the turbulence in streets and street intersections are modelled by parametric
62 relations on the network, while the concentration in the streets is estimated by a mass flow balance.
63 Street network models have proven to be efficient for rapid prediction of air quality over large urban
64 domains (Kakosimos et al., 2010; Soulhac et al., 2011).

65 Fellini et al., 2019 developed a propagation model on networks to simulate pollutant dispersion from
66 a point source using the same geometrical description as street network models. They used tools and
67 metrics from complex network theory (Fellini et al., 2020, 2021) to unveil the physical mechanisms
68 that drive dispersion processes and to detect vulnerable locations where a toxic gaseous release can

69 cause the greatest impact. In this paper, a similar methodology is used to predict the optimal location
70 to reduce traffic emissions.

71 The theory of complex networks aims to describe a system as a network of interactions between its
72 elements. These elements are represented by nodes, interconnected by links whenever a relationship
73 is observed between the corresponding elements. The resulting network can then be described by
74 means of multiple metrics or used as a basis for modelling. This theory has been successfully adopted
75 in the field of urban science to investigate the topological properties of cities but also mobility patterns
76 of citizens and socio-economic dynamics (Batty, 2013; Barthelemy, 2016). Recently, the complex
77 network approach has proved useful in the study of geophysical flows, for example to analyse the
78 motion of particles in turbulent flows (Iacobello et al., 2019; Ser-Giacomi et al., 2019).

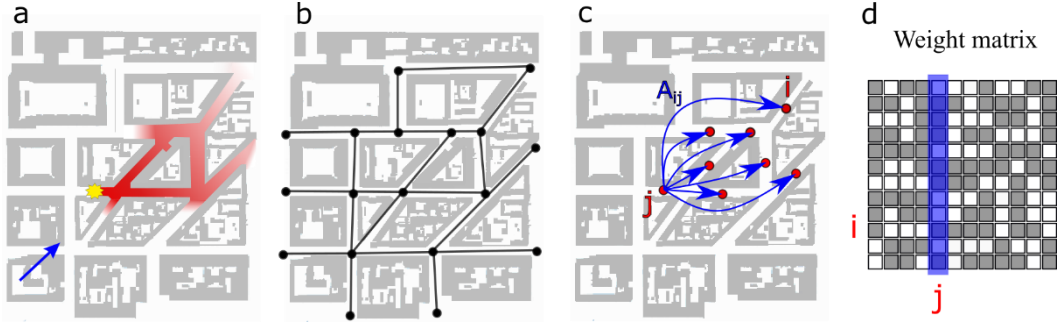
79 Given the complexity of transport and transformation processes of pollutants in the urban
80 atmosphere and the multiplicity of meteorological, emission and exposure scenarios, we propose in
81 this work a network approach to model the relation between pollutant emissions and their impact on
82 citizens and to perform source apportionment analyses. The aim is to answer the question: if a
83 borough would like to reduce emissions in a neighborhood by a certain percentage, on which streets
84 should action be taken in order to maximise the reduction in citizen's exposure? It will be
85 demonstrated that due to the representation of emissions, air quality and exposure in the form of a
86 complex network, multiple emissions and exposure scenarios can be easily simulated and the
87 fundamental elements of the phenomenon are clearly identified.

88 The work is organized as follows: in section 2 the construction of the network is outlined together with
89 the fundamental concepts of the model. Section 3 presents the case study to which the methodology
90 is applied. Section 4 shows the potential of the model when dealing with a passive pollutant. In section
91 5, the method is extended to study exposure to reactive pollutants. Finally, in section 6, the
92 conclusions and perspectives of the work are presented.

93 2. Methodology

94 2.1 Complex network representation

95 A weighted and directed network (Boccaletti et al., 2006) is adopted to model the correlation between
96 pollutant emissions and concentration in the streets. In classical street network models, the network
97 mimics the geometry of the urban fabric, with streets represented as links connecting two nodes that
98 correspond to street intersections (Figure 1.a). Conversely, nodes represent here the streets while the
99 directed links are the emission-impact relation between streets. Therefore, distant streets can also be
100 connected (Figure 1.c) differently from the physical network of streets that is limited by the urban
101 shape. The structure of the network is mathematically described by the adjacency matrix whose
102 elements have a value equal to 1 or 0 depending on whether the pairs of nodes are connected or not
103 in the graph. In addition to this information, the weight matrix A expresses for each non-zero value
104 the weight (i.e. the importance) associated with the connection (Figure 1.d). The link weights
105 therefore contain all the information relating to the transport of pollutants from one street to another.



106

107 *Figure 1: Schematic representation of pollutant dispersion in a dense city (a), the classical street-network domain (b), the*
 108 *emission-concentration network considered in this work (c) and the corresponding weight matrix (d). The non-zero elements*
 109 *in the blue column collect the concentration values in the contaminated streets from node j .*

110 The main assumption underlying this work is that to first order, the transport within and between the
 111 streets can be represented as:

$$\mathbf{C} = \mathbf{A}\mathbf{Q} \quad (1)$$

112 where \mathbf{Q} and \mathbf{C} are the emission and concentration in each street respectively, and A_{ij} is an entry of
 113 the weight matrix that represents how emissions in street j result in concentrations in street i .
 114 Denoting the number of streets by N , A is of size $N \times N$. Eq. (1) assumes that there is a linear relation
 115 between emissions and concentration, which is a hypothesis that will be tested later in the paper.
 116 Chemistry will create a nonlinear relation between \mathbf{Q} and \mathbf{C} . This issue will be dealt with in Section 5.
 117 We note that Eq. (1) is equivalent to a source apportionment method as each row of A represents the
 118 linear weights of the sources contributing to the concentration in a street of the network.

119 2.2 Construction of the weight matrix A

120 The weight matrix A in Eq. (1) is constructed using the model SIRANE. SIRANE is an operational street
 121 network model for urban dispersion that has been adopted in several European cities and has been
 122 validated against both wind tunnel experiments and field campaigns (Carpentieri et al., 2012; Soulhac
 123 et al., 2003, 2012, 2017). The model is based on a simplified description of the urban geometry and
 124 adopts parametric relations to simulate the transport mechanisms of pollutants within the urban
 125 canopy. The streets of a city district are modelled as a network of boxes within which the pollutant is
 126 assumed to be uniformly mixed. The model simulates three main transport mechanisms: advection
 127 along the street axis (Q_{adv}), turbulent vertical exchange at the interface between the street and the
 128 overlying atmosphere ($Q_{H,turb}$), and exchange at street intersections (Q_I). The main physico-chemical
 129 processes are also modelled. These are the null-cycle chemistry and wet (Q_{wash}) and dry deposition
 130 (Q_{part}). The mass balance over each street volume for a passive scalar can be written as:

$$Q + Q_I = Q_{H,turb} + Q_{adv} + Q_{part} + Q_{wash}. \quad (2)$$

131 Above roofs, a Gaussian plume model is used. The interaction between the dispersion above roof and
 132 inside the street is mainly taken into account in the term $Q_{H,turb}$. SIRANE requires as input data the
 133 urban geometry, the meteorological conditions of the site, the background concentration of pollutants
 134 and the emissions within the streets. A meteorological pre-processor utilises parametrisations to
 135 simulate the boundary layer above roofs from the assigned conditions (Soulhac et al., 2011).

136 To construct the weight matrix A , we perform simulations with SIRANE on the urban district that will
 137 be presented in Section 3. We assume that the background concentration is zero and that the only
 138 polluting source in the streets is the release of a gas behaving like a passive scalar. This is achieved
 139 using an ozone (O_3) emission in SIRANE, which, without the presence of any NO and NO_2 , is an inert

140 tracer in the model. We perform the simulations at a single wind speed U and one wind direction ϕ
 141 at a time. Under these assumptions, the j -th column of the weight matrix (Figure 1.c-d) is filled by
 142 simulating a unit ozone emission in the j -th street of the network. The resulting concentration values
 143 in street network provides column j of matrix A . By repeating this operation for all the streets of the
 144 network, A is obtained. This procedure is then repeated for 8 wind directions, and A therefore
 145 depends on the intensity and direction of the wind above roofs, i.e. $A = A(U, \phi)$. In practice, A is
 146 determined for one wind speed only, which we will refer to as the reference velocity U_0 and associated
 147 weight matrix A_0 . The physics of the problem can be used to infer A at other wind speeds (see section
 148 4.2).

149 2.3 Exposure

150 To find the best place to reduce emissions in the urban district, a metric is required that quantifies the
 151 exposure of citizens. Personal exposure depends sensitively on the type of pollutant, inhalation rate
 152 and duration of the exposure. Here, we adopt a simple measure for the exposure in a street e_i [g/hr]
 153 as:

$$154 \quad e_i = p_i C_i q, \quad (3)$$

155 where p_i is the number of people living in street i (note that summation over repeated indices is not
 156 implied here) and q is the inhalation rate of a person, which is taken to be $0.571 \text{ m}^3/\text{hr}$ (Epa & Factors
 157 Program, 2011). In matrix notation, this can be written as

$$158 \quad \mathbf{e} = \mathbf{q}\mathbf{p} \circ \mathbf{C} = \mathbf{q}\mathbf{p} \circ \mathbf{A}\mathbf{Q} = \mathbf{E}\mathbf{Q}, \quad (4)$$

159 where \circ is the Hadamard product and $E_{ij} = qp_i A_{ij}$ is the exposure matrix. In this work, we will
 160 assume that the number of people p_i is constant as a function of time, but note that it is
 161 straightforward to consider different, more complex, scenarios (different days of the week, different
 162 hours) by changing the \mathbf{p} vector only.

162 2.4 Street population estimation

163 To estimate the number of citizens in each street (p_i), we assume that the street is flanked by two
 164 buildings of constant width w , of length equal to the length of the street (L_i), and of height equal to
 165 the average depth of the street canyon H_i (panel c in Figure 2). We then assume a constant storey
 166 height H_F to assess the number of floors. The total living space for a street is thus given by:

$$167 \quad S_i = 2 \frac{H_i L_i w}{H_F}. \quad (5)$$

168 The corresponding resident population (p_i) can be calculated as the ratio between the living space
 169 and the average area per capita S_p , i.e. the average living space for a resident. This latter can be
 170 evaluated for a specific district as the ratio of the total living area given by the buildings in the district
 171 $\sum_j 2 H_j L_j w / H_F$ and the number of citizens n_{TOT} living in the district. Assuming a constant width for
 172 the buildings, we obtain the following expression for the number of people in street i :

$$173 \quad p_i = 2 \frac{H_i L_i w}{H_F} \frac{n_{TOT}}{2 w \sum_j H_j L_j / H_F} = \frac{H_i L_i}{\sum_j H_j L_j} n_{TOT}. \quad (6)$$

173 3. South Kensington case study

174 The case study (latitude 51.4998, longitude -0.1748) is located in South Kensington, a district west of
 175 central London, UK (Figure 2). The study area spans $672 \times 1344 \text{ m}^2$ between Hyde Park and South

176 Kensington station and is characterized by high population, developed transport and dense buildings.
177 The high variety of morphological features (e.g., length of the streets, height of the buildings) and the
178 different population density of the building blocks make this area suitable for investigating which
179 places are most sensitive to the reduction of polluting emissions.

180 The representation of the urban district in SIRANE is detailed in Grylls et al., 2019. The street network
181 is composed of 46 streets that are represented as straight links with starting and ending points located
182 at the centre of the connecting intersections. Consistent with the description of the street as a box
183 (see Section 2.2), each street has average geometric properties associated with it. The height (H) is
184 given by the average height of the side buildings, while the street width (W) is the average distance
185 between the lateral buildings (see Figure 2). Street length (L) is simply the distance between the two
186 street intersections.

187 The geometrical properties of the street canyons are used to estimate the resident population
188 according to Eq. (6). The total number of citizens n_{TOT} is estimated as the product of the district area
189 and the average population density ($12876 \text{ peo}/\text{km}^2$) of the reference region (Kensington and
190 Chelsea) derived from Park (2020).

191 To construct the matrix A for the study area, the simulations with SIRANE are performed with typical
192 meteorological conditions: a temperate night ($T = 4 \text{ }^\circ\text{C}$) in neutral stability conditions with cloud
193 cover (5 Oktas) and no precipitation. The night condition is adopted to simulate the dispersion of
194 ozone as a passive scalar (see Section 2.2). Starting from these assigned conditions, SIRANE uses
195 parametrizations to estimate the characteristic properties of the boundary layer as well as the reaction
196 rates for reactive pollutants (see Section 5).

197 Vehicular emissions in the streets are estimated through the coupling of a VISSIM traffic
198 microsimulation (Bloomberg & Dale, 2000) and the emission model developed by Int Panis et al.
199 (2006). The resulting second-by-second NO_x emissions are time averaged over 1 hour and spatially
200 averaged over the street boxes. Details are provided in Grylls et al. (2019).

201 For the passive scalar analysis, the background concentration was taken equal to zero (see also Section
202 2.1). For the reactive scalar analysis, realistic background concentrations were used. These were
203 obtained as the average value in the 2021 for the reference region (Kensington and Chelsea): $\text{NO}_2 =$
204 $34.26 \mu\text{g}/\text{m}^3$, $\text{NO} = 17.09 \mu\text{g}/\text{m}^3$ (UK Ambient Air Quality Interactive Map), $\text{O}_3 = 27.31 \mu\text{g}/\text{m}^3$
205 (Greater London Authority). It is worth noting that the ozone estimate is an eight-hour average. To
206 simulate photochemical reactions, a sunny day ($T=14 \text{ }^\circ\text{C}$) at noon was considered in this case.

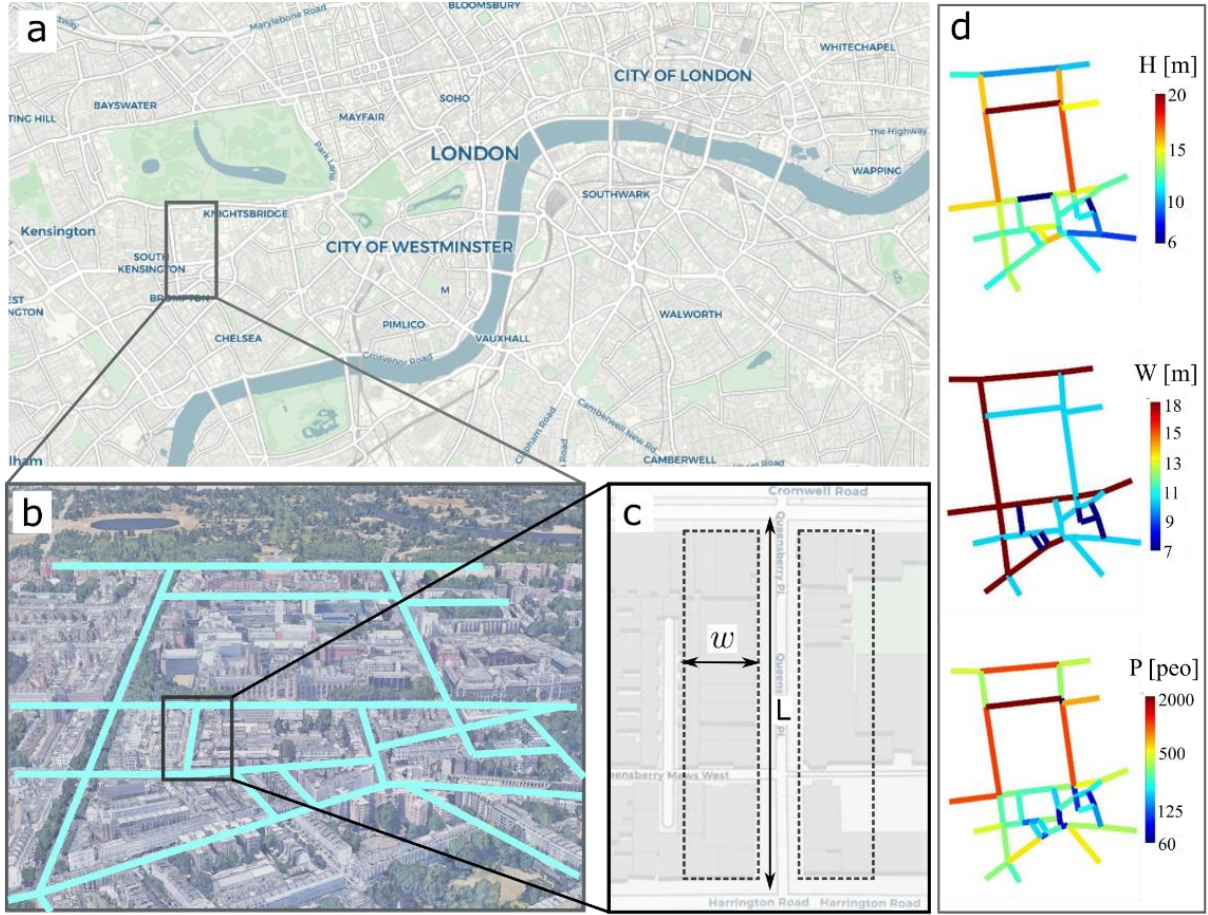


Figure 2: a) Location of South Kensington district in Central London. b) The study area and its street network. c) Schematization of lateral buildings for the estimation of the population. d) Depth (H) and width (W_s) of the street canyons and estimated population in the streets (P).

207
208
209
210

211 4. Passive scalar transport

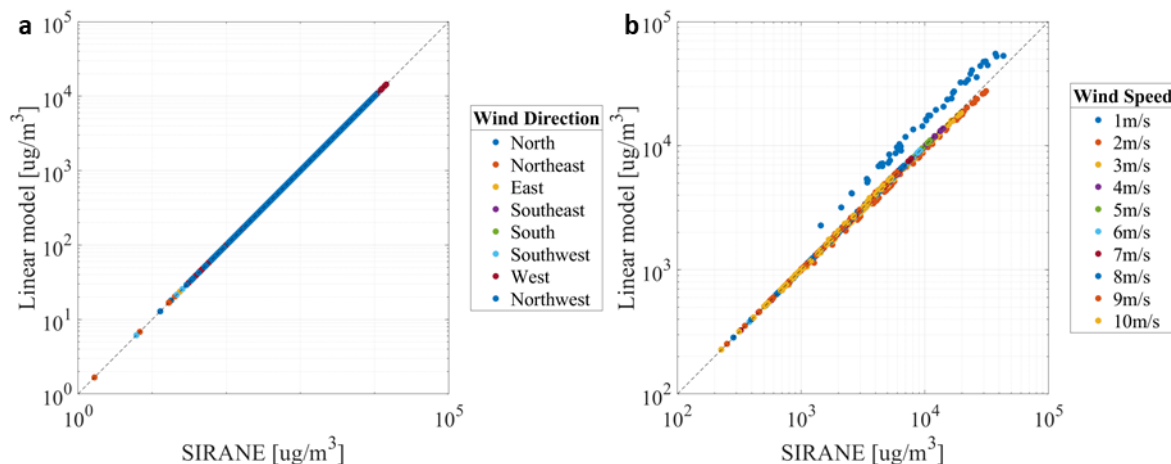
212 4.1 Concentration reconstruction

213 Following the method explained in Section 2.2, we construct the weight matrix A for the South
214 Kensington district for eight different wind directions, assuming a constant wind speed $U_0=5$ m/s. In
215 order to verify whether the resulting matrix is correct, we then perform a simulation in SIRANE with
216 random emissions in multiple streets simultaneously (i.e. a random Q vector) and we compare the
217 results with the concentration in the streets estimated using the linear model presented in Eq. (1).
218 This comparative test is repeated 20 times and the results are reported in Figure 3(a), where each
219 point represents the concentration in a single street for a specific wind direction and for an initial
220 random distribution of emissions. The results show an excellent match between the two models and
221 suggest that the linear assumption holds in the case of passive pollutants emitted in a rainless day (i.e.
222 neglecting chemical reactions and dry and wet deposition) and with negligible re-entrainment of
223 pollutants dispersed above roof levels. In fact, in this case the balance in Eq. (2) can be rewritten as:

$$Q + Q_I = Q_{H,turb} + Q_{adv} \rightarrow Q + U_S W H C_{up} = u_d W L C + U_S W H C, \quad (7)$$

224 where U_S and u_d are the advective velocity along the street canyon and the rate of vertical turbulent
225 transfer at roof level, C and C_{up} are the average concentration in the street and in the airflow entering
226 the street from the upwind intersection. The latter is in turn given by a linear superposition of the

227 emissions in the upwind streets. These considerations evidence that the balance in Eq. (7) can be
 228 formulated as Eq. (1) and validate the very good correlation in Figure 3(a).



229

Figure 3: a) Concentration in the streets predicted by SIRANE and by the linear model proposed in Eq. (1) for different wind direction and a constant wind intensity (5 m/s). b) Accuracy as a function of wind speed.

230 4.2 Wind speed correction

231 As highlighted by Eq. (7), the wind intensity affects the pollutant balance in the street by means of the
 232 two characteristic velocities U_S and u_d . Both these velocities can be parameterized as linear functions
 233 of the friction velocity (u_*) of the overlying boundary layer (Salizzoni et al., 2009 and Soulhac et al.,
 234 2010). Furthermore, assuming that the weather conditions are constant over the area of interest, the
 235 ratio between u_* and the free stream velocity (U) of the boundary layer is constant. These
 236 considerations suggest that matrix A in Eq. (1) is inversely proportional to the wind intensity U .
 237 Therefore, we can generalise the weight matrix A for a general wind speed as:

$$A(U, \phi) = \frac{U_0}{U} A_0(U_0, \phi) \quad (8)$$

238 where U_0 is the reference velocity (5 m/s in this study) and A_0 is the corresponding weight matrix.
 239 This scaling is adopted to simulate scenarios with ten different wind intensities, by using Eqs. (1) and
 240 (8). As for the reference case, random emissions Q are prescribed in the streets. The concentration
 241 predictions of Eq. (8) are compared in Figure 3(b) with the outcomes of the simulations performed
 242 with SIRANE. For each wind intensity, we take the average over the eight wind directions (ϕ). At low
 243 wind speed, the dispersion of pollutants above roof level has a significant impact. For very low wind
 244 speeds, the pollution transport above the streets via plumes become important which do not scale as
 245 Eq. (8); this leads to inaccuracies in the proposed approximation.

246 4.3 Diagonal dominance of A

247 In this section we explore the diagonal dominance of matrix A , which is satisfied when
 248 $|A_{ii}| / \sum_{j \neq i} |A_{ij}| > 1$, i.e. the matrix is diagonally dominant when, for each row, the magnitude of the
 249 diagonal element in a row is larger than or equal to the sum of the magnitudes of all the other entries in
 250 that row. If A is found to be diagonally dominant, the concentration in the streets is mainly affected
 251 by local emissions. It should be noted that $|A_{ii}| / \sum_{j \neq i} |A_{ij}|$ tends to infinity as the matrix becomes
 252 diagonal. Therefore, to obtain a useful measure for the matrix as a whole, the harmonic mean of
 253 $|A_{ii}| / \sum_{j \neq i} |A_{ij}|$ for all the rows is taken:

$$D = \left(\frac{1}{N} \sum_i \frac{\sum_{j \neq i} |A_{ij}|}{|A_{ii}|} \right)^{-1}. \quad (9)$$

254 If $D > 1$ then the matrix is diagonally dominant on average. The harmonic mean weighs the smallest
 255 row values highest and will thus be a conservative estimate. By calculating D for all eight wind
 256 directions, we find that $133 < D < 193$, and thus conclude that self-interactions are expected to be
 257 very strong. Substitution of Eq. (8) shows that D is independent of wind velocity (provided the wind
 258 speed is not too small).

259

260 4.4 Reducing network complexity

261 The network contains a large number of links due to the transport of pollutants out of street canyons
 262 via the atmosphere and into street canyons downwind. The pollutant plume dilutes rapidly with
 263 downstream distance, resulting in a large number of very weak links. These can be removed without
 264 a noticeable impact on the concentration predictions. As demonstrated in the previous section, the
 265 matrix A is diagonally dominant, and we can use the mean of the diagonal entries to quantify the
 266 dominant interactions. We select a geometric mean $(\prod_1^N A_{ii})^{\frac{1}{N}}$ to avoid one street dominating the
 267 mean as the diagonal entries can vary greatly in magnitude depending on the street properties.
 268 Introducing a threshold value α , the modified weight matrix \check{A}_{ij} is determined as:

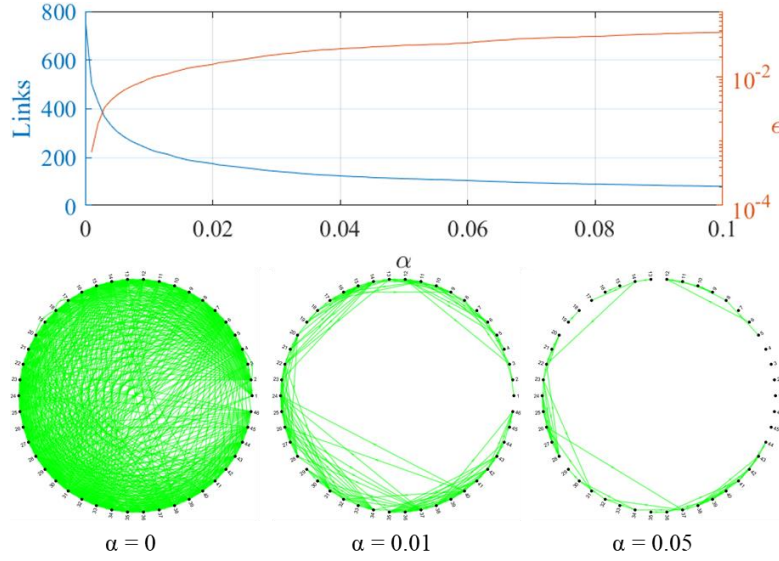
$$\check{A}_{ij} = \begin{cases} A_{ij}, & \text{if } A_{ij} > \alpha \left(\prod_1^N A_{ii} \right)^{\frac{1}{N}} \\ 0, & \text{otherwise} \end{cases} \quad (10)$$

269

270 Figure 4 (blue curve) shows the trend in the number of links of matrix \check{A}_{ij} as a function of α : using a
 271 threshold value $\alpha = 0.01$ decreases the number of links by a factor 3.28. To quantify the error made
 272 due to link removal, we consider the relative error in the predicted concentration:

$$273 \quad \epsilon = \frac{\|\mathbf{c} - \check{\mathbf{c}}\|_2}{\|\mathbf{c}\|_2} = \frac{\|(A - \check{A})\mathbf{Q}\|_2}{\|A\mathbf{Q}\|_2} \approx \frac{\|A - \check{A}\|_2}{\|A\|_2}$$

274 where $\|\cdot\|_2$ is the L_2 -norm, and the last step involves a change from a vector norm to a matrix norm.
 275 The red curve in Figure 4 evidence that the relative error ϵ is about 0.01 at $\alpha = 0.01$, and 0.05 at $\alpha =$
 276 0.1. This demonstrates that the number of links can be reduced severely without significantly altering
 277 the properties of A . For large networks, using a small threshold value α will imply substantial savings
 278 in memory and an increase in computational performance. However, since the network considered
 279 here is small, we will not make use of the simplification.



280

281

Figure 4: Number of links and error (ϵ) due to link removal for networks with different exclusive threshold α .

282 4.5 Where to reduce emissions?

283 The scenario considered here is that a borough decides to reduce its total emissions by a certain
 284 amount and would like to know in which street this should be done in order to have the largest health
 285 benefits for its citizens. To answer this question, it is necessary to quantify the contribution of the
 286 emission in each street to the air pollution in the urban area. The process of evaluating the effect of a
 287 single source on the total concentrations is called source apportionment.

288 Following the source apportionment strategy, and in particular the tagged species approach (Wang et
 289 al., 2009; Grewe et al., 2010), we perturb the emission-exposure model introduced in Section 2 to
 290 analyse the exposure variation due to a change in the pollutant emissions as:

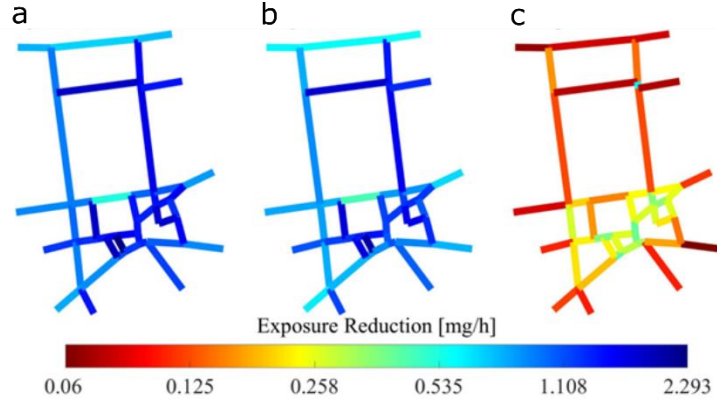
291

$$\delta \mathbf{e} = E \delta \mathbf{Q}. \quad (11)$$

292 The desired emission change is assumed to be $\delta Q = b \bar{Q}$ where $\bar{Q} = \frac{1}{N} \sum_i Q_i$ is the average emission
 293 rate per street and b is a parameter, which is taken to be 0.10 here. We are looking for the street j
 294 whose emission reduction $-\delta Q$ maximizes the sum of the exposure change in all the streets. The total
 295 exposure reduction R_j due to an emission reduction $\delta Q_j = -\delta Q$ in street j can be expressed by:

$$R_j = - \sum_i \delta e_i = - \sum_k \delta Q_k \sum_i E_{ik} = \delta Q \sum_i E_{ij} \quad (12)$$

296 where the last step uses that $\delta \mathbf{Q}$ is different from 0 only in street j . Note that $\sum_i E_{ij}$ is the outdegree
 297 of node j (d_j^+) (Newman, 2010). So, the optimal place to reduce emissions corresponds to the node
 298 with the highest outdegree in the defined weighted network.



299

300
301
302

Figure 5: Exposure reduction achieved by decreasing the emission in the street by a constant quantity δQ . Panels a and b show the maximum and average values for the different wind directions. Panel c shows the average computed by neglecting self-interactions.

303
304
305
306
307
308
309
310
311
312
313

The exposure reduction (\mathbf{R}) is shown in Figure 5. In the analysis, we consider a single wind intensity $U_0 = 5$ m/s since we are interested in the variability of \mathbf{R} among the streets and not in its absolute value. In this sense, the results shown in Figure 5 are also valid for the other wind intensities, in accordance with the linear relation in Eq. (8). Panels a and b show the maximum and average \mathbf{R} for the different wind direction scenarios. The similarity between the two figures suggests that the results depend only weakly on the wind direction. This is likely because the main exposure reduction occurs in the same street where the emission is limited since matrix A (and thus E) is strongly diagonally dominant, as was shown in Section 4.3. To clarify this point, we report in panel c the results obtained by neglecting self-interactions in matrix E , i.e. for each street we compute the exposure reduction that is achieved in the whole network except in the street where the emission is reduced. The value of \mathbf{R} is considerably lower in this case, confirming the importance of self-interactions.

314
315
316

The variability in the exposure reduction among the streets can be related to the geometry of the street canyons and their connectivity. When only self-interactions are considered (panel a and b), Eq. (12) can be evaluated exactly:

$$R_i = \delta Q E_{ii} = \delta Q q p_i \frac{U_0}{U} A_{0,ii} = \frac{U_0}{U} \frac{\delta Q q p_i}{u_{d0} W_i L_i} = \frac{U_0}{U} \frac{\delta Q q n_{TOT} H_i}{u_{d0} \sum_j H_j L_j W_i} \quad (13)$$

317

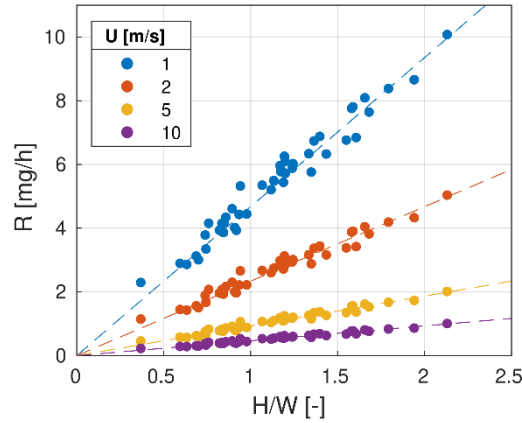
318
319
320
321
322
323
324
325
326
327
328

The exposure reduction will be higher the higher the E_{ii} entry. This increases with the resident population in the street (p_i) and with the entry A_{ii} which provides the increase in pollutant concentration per unit emission. According to Eq. (6), p_i is a linear function of the length of the street and the height of the buildings. Following the model reported in Eq. (7) and considering that there is no pollutant exchange at street intersections, we find that A_{ii} (here reported for a general wind intensity, i.e. $A = A_0 U_0 / U$) decreases with W and L . Consequently, as demonstrated in Eq. (13), the exposure reduction is expected to scale with the street aspect ratio H/W , while the contribution of the street length should be negligible. This is confirmed by Figure 6, which shows a linear trend of the exposure reduction with the canyon aspect ratio for the different scenarios of wind intensity (U). The dashed lines correspond to the prediction in Eq. (13). Panels a and b of Figure 5 evidence that R_j is not dependent on the street length.

329
330
331
332

When self-interactions are neglected (panel c), the exposure reduction in Eq. (12) is high when E_{ij} is different from zero for many j , i.e., when the interconnectivity of the network is high. For this reason, the largest exposure reductions in panel c are obtained on the well interconnected streets of the network.

333



334

335 *Figure 6: Exposure reduction (average over the wind directions) as a function of the aspect ratio (H/W) of the streets.*
 336 *Dashed lines correspond to the prediction in Eq. (13),*

337

338 5. Extension to photochemical smog

339 The formalism will now be extended to include chemically reacting species, namely the NO – NO₂ –
 340 O₃ cycle associated with photochemical smog (Oke et al., 2017). We follow SIRANE by assuming that
 341 the characteristic time scales of the chemical reactions are small compared to the residence time of
 342 pollutants within the streets. Under this assumption, a two-step method can be used to model the
 343 fate of the chemical species. First, we consider that ozone, nitric oxide and nitrogen dioxide are
 344 transported passively across the street network. After reaching the designated street, we assume that
 345 the species are in a photochemical steady state inside the canyon, and we apply chemical reactions to
 346 obtain the final concentration.

347 Adopting the network approach, the first step is the passive redistribution of chemical species, given
 348 by

$$\tilde{c}_{NO_2} = A\mathbf{Q}_{NO_2}, \quad \tilde{c}_{NO} = A\mathbf{Q}_{NO}, \quad \tilde{c}_{O_3} = A\mathbf{Q}_{O_3}. \quad (14)$$

349

350 Written in a single matrix multiplication, this becomes

$$\begin{bmatrix} \tilde{c}_{NO_2} \\ \tilde{c}_{NO} \\ \tilde{c}_{O_3} \end{bmatrix} = \begin{pmatrix} A & 0 & 0 \\ 0 & A & 0 \\ 0 & 0 & A \end{pmatrix} \begin{bmatrix} \mathbf{Q}_{NO_2} \\ \mathbf{Q}_{NO} \\ \mathbf{Q}_{O_3} \end{bmatrix}, \quad \text{or simply } \tilde{\mathbf{c}} = B\mathbf{Q}. \quad (15)$$

351 The second step is to apply the chemistry which can be represented by

$$\mathbf{c} = \mathbf{f}(\tilde{\mathbf{c}}), \quad (16)$$

352 where \mathbf{f} is a nonlinear function that maps $\tilde{\mathbf{c}}$ to \mathbf{c} in each street. The null-cycle chemistry (Oke et al.,
 353 2017) together with the conservation of N and O species in a single street results in the following
 354 equilibrium concentrations:

$$[O_3] = \frac{-(k_3(c_N - c_O) + k_1) + \sqrt{\Delta}}{2k_3},$$

$$\begin{aligned} [\text{NO}_2] &= c_O - [\text{O}_3], \\ [\text{NO}] &= c_N - [\text{NO}_2] = c_N - c_O + [\text{O}_3], \end{aligned} \quad (17)$$

355 where

$$\begin{aligned} c_N &= [\widetilde{\text{NO}}] + [\widetilde{\text{NO}}_2] + [\text{NO}]_b + [\text{NO}_2]_b, \\ c_O &= [\widetilde{\text{NO}}_2] + [\widetilde{\text{O}}_3] + [\text{NO}_2]_b + [\text{O}_3]_b, \\ \Delta &= (k_3(c_N - c_O) + k_1)^2 + 4k_1k_3c_O. \end{aligned} \quad (18)$$

356 Here, the brackets denote molar concentrations, that are linked to the mass concentrations as $\widetilde{X} =$
 357 $M_X[X]$, where M_X is the molar mass (g/mol) of species X . k_1 is the rate (expressed in $\text{m}^3\text{mol}^{-1}\text{s}^{-1}$) of
 358 NO_2 regeneration from NO and O_3 reaction, and k_3 is the photolysis rate of NO_2 (expressed in s^{-1}).
 359 Denoting $\widetilde{\mathbf{c}} = [\widetilde{\text{NO}}, \widetilde{\text{NO}}_2, \widetilde{\text{O}}_3]^T$ and $\mathbf{c} = [\text{NO}, \text{NO}_2, \text{O}_3]^T$ as the mass concentration vectors in a single street
 360 before and after the chemical reaction, respectively, the relation between the two can be expressed
 361 as

$$\mathbf{c} = \mathbf{f}_s(\widetilde{\mathbf{c}}) = \mathbf{f}_s(\widetilde{\text{NO}}, \widetilde{\text{NO}}_2, \widetilde{\text{O}}_3), \quad (19)$$

362

363 where \mathbf{f}_s represents \mathbf{f} for a single street. There are a few specifics of air quality simulations that
 364 simplify the calculation of the term \mathbf{f}_s . First, ozone is a secondary pollutant, which implies that it is
 365 formed from reactions with primary pollutants and thus $\mathbf{Q}_{\text{O}_3} = \mathbf{0}$, which in turn implies that $\widetilde{\text{O}}_3 = 0$
 366 (see Eq. (14)). Second, the emissions of NO and NO_2 are typically prescribed in terms of an emission
 367 ratio $a = Q_{\text{NO}_2}/Q_{\text{NO}_x}$ where a is a constant and Q_{NO_x} is reported on a NO_2 basis (i.e. it is assumed
 368 that all NO is converted to NO_2). This means that

$$\mathbf{Q}_{\text{NO}} = (1 - a) \frac{M_{\text{NO}}}{M_{\text{NO}_2}} \mathbf{Q}_{\text{NO}_x}, \quad \mathbf{Q}_{\text{NO}_2} = a \mathbf{Q}_{\text{NO}_x}, \quad (20)$$

369

370 and, because of the linearity of A , that $\widetilde{\text{NO}} = (1 - a) \frac{M_{\text{NO}}}{M_{\text{NO}_2}} \widetilde{\text{NO}}_x$ and $\widetilde{\text{NO}}_2 = a \widetilde{\text{NO}}_x$. Thus, we can write

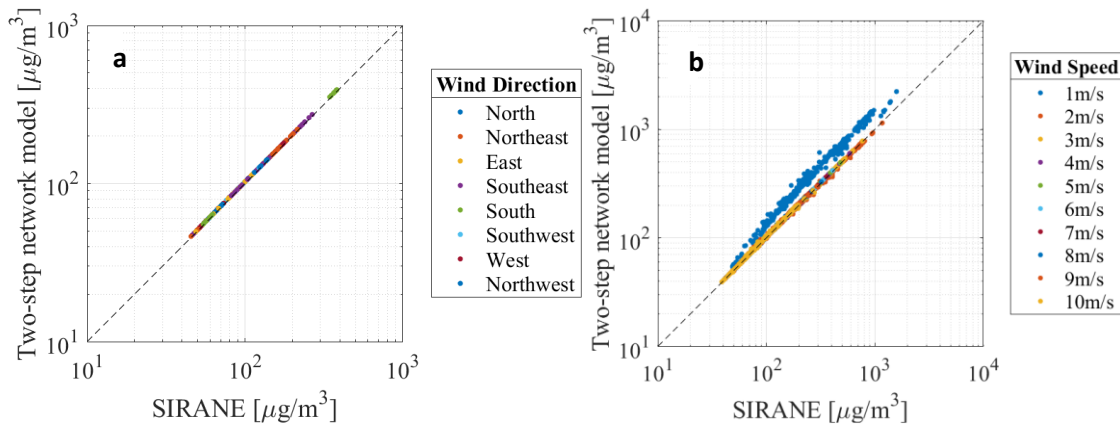
$$\mathbf{c} = \mathbf{f}_s(\widetilde{\text{NO}}, \widetilde{\text{NO}}_2, \widetilde{\text{O}}_3) = \mathbf{g}(\widetilde{\text{NO}}_x), \quad (21)$$

371

372 where \mathbf{g} is a function that depends on the $\widetilde{\text{NO}}_x$ concentration only.

373 To verify the two-step network model introduced above, we compare it with SIRANE. We note that
 374 also the chemical model currently implemented in SIRANE derives from the same assumptions
 375 (photostationary equilibrium in the canyon and NO and O balance). However, differently from
 376 SIRANE, we neglect the deposition of chemical species and all the dynamics of dispersion and
 377 transformation above roof levels. These assumptions are made to maintain a clear mathematical
 378 formulation, in line with the network description. In fact, the fate of the three species is predicted
 379 simply by using Eq. (15), i.e. matrix A from the passive scalar model, and by applying the function \mathbf{g}
 380 for the chemical transformations. To compare the two models, we simulate random emissions of NO_x
 381 in multiple streets and we compare the resulting concentrations. An emissions ratio $a = 0.2$ was
 382 assigned to the emissions in both models (Carslaw et al., 2016; O'Driscoll et al., 2016; UK National
 383 Atmospheric Emission Inventory, 2018). The linear scaling (Eq. (8)) for the wind intensity was used to
 384 simulate different speed scenarios starting from a single matrix reconstruction (A_0 for $U_0 = 5$ m/s).
 385 We find that even in the case of chemical species, the concentrations are predicted with great
 386 accuracy for different wind directions and intensities (Figure 7). Although it is not visible from Figure

387 7.a, the two-step network model gives a slightly higher prediction than SIRANE, about 2% in this data
 388 set. These slight deviations are because SIRANE takes into account the deposition of nitrogen oxides
 389 while the matrix A is constructed for a non-depositing passive scalar (see Section 2.2).



391 *Figure 7: Concentration of NO₂ in the streets predicted by SIRANE and by the two-step network model introduced in Eqs.*
 392 *(15)-(21). The comparison is made for simulations with different a) wind directions b) and wind speeds.*

393 5.1 Calculation of emission sensitivity

394 The inclusion of chemistry makes the exposure (Section 2.3) a nonlinear function of the emissions \mathbf{Q} :

$$395 \mathbf{e} = \mathbf{q}\mathbf{p} \circ \mathbf{C} = \mathbf{q}\mathbf{p} \circ \mathbf{f}(\tilde{\mathbf{C}}) = \mathbf{q}\mathbf{p} \circ \mathbf{f}(B\mathbf{Q}). \quad (22)$$

396 Exposure variation in the streets due to a change in the pollutant emissions can be expressed as

$$397 \delta \mathbf{e} = \mathbf{p} \circ \delta \mathbf{C} = \mathbf{p} \circ \delta \mathbf{f}(B\mathbf{Q}), \quad (23)$$

398 and a Taylor series expansion around the reference emissions \mathbf{Q}_0 results in

$$399 \delta \mathbf{e} = \mathbf{e} - \mathbf{e}_0 \approx \mathbf{q}\mathbf{p} \circ \frac{\partial \mathbf{f}}{\partial \tilde{\mathbf{C}}} B \delta \mathbf{Q}, \quad (24)$$

400 or simply

$$401 \delta \mathbf{e} = E \delta \mathbf{Q} \quad \text{where} \quad E = \mathbf{q}\mathbf{p} \circ \frac{\partial \mathbf{f}}{\partial \tilde{\mathbf{C}}} B. \quad (25)$$

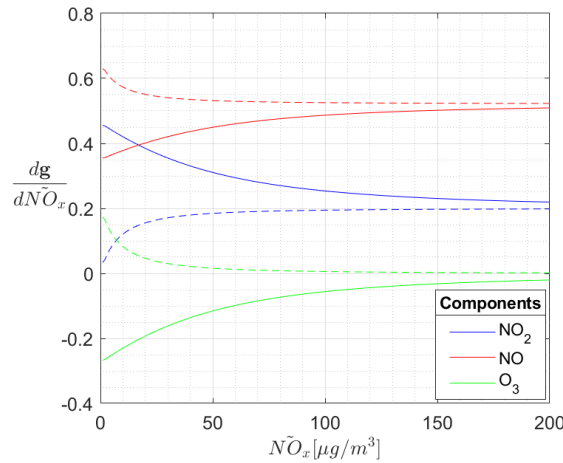
402 Recalling that function \mathbf{f} for a single street is denoted \mathbf{f}_s for and that it can be simplified to \mathbf{g}
 403 according to Eq. (21), the Jacobian is given by

$$404 \frac{\partial \mathbf{f}_s}{\partial \tilde{\mathbf{c}}} = \begin{pmatrix} \frac{\partial f_{s,1}}{\partial \tilde{c}_1} & \frac{\partial f_{s,1}}{\partial \tilde{c}_2} & \frac{\partial f_{s,1}}{\partial \tilde{c}_3} \\ \frac{\partial f_{s,2}}{\partial \tilde{c}_1} & \frac{\partial f_{s,2}}{\partial \tilde{c}_2} & \frac{\partial f_{s,2}}{\partial \tilde{c}_3} \\ \frac{\partial f_{s,3}}{\partial \tilde{c}_1} & \frac{\partial f_{s,3}}{\partial \tilde{c}_2} & \frac{\partial f_{s,3}}{\partial \tilde{c}_3} \end{pmatrix} = \frac{d\mathbf{g}}{d\tilde{\mathbf{N}}_x} \begin{pmatrix} (1-a) \frac{M_{\text{NO}}}{M_{\text{NO}_2}} & a & 0 \end{pmatrix} \quad (26)$$

405

401 Figure 8 shows the sensitivity $d\mathbf{g}/d\tilde{\mathbf{N}}_x$ for the photochemical equilibrium. Solid lines represent the
 402 model feedback when the background concentrations of the case study are considered. Dashed lines
 403 refer to the scenario with zero background concentrations. The starting position of the three
 404 component curves depends on the background concentration, while the asymptotic value for high
 405 $\tilde{\mathbf{N}}_x$ concentration depends on the emission ratio a , i.e. when the emitted and advected nitrogen

406 oxides (\widetilde{NO}_x) are very large, the background concentrations become negligible and the model behaves
 407 linearly (constant $d\mathbf{g}/d\widetilde{NO}_x$). We observe that $d\mathbf{g}/d\widetilde{NO}_x$ for ozone may be negative or positive. The
 408 negative(positive) $d\mathbf{g}/d\widetilde{NO}_x$ occurs when the background concentration of ozone ($[O_3]_b$) is
 409 higher(lower) than the ozone concentration at equilibrium ($[O_3]$). In any case, the rate of change of
 410 ozone always approaches zero as NO_x increases. This is due to the consumption of available ozone by
 411 nitrogen oxides and can be derived from equations (17)-(18) showing that $[O_3]$ goes to zero when \widetilde{NO}_x
 412 tends to infinity. Finally, we remark that for the case study considered here, the ozone consumption
 413 decreases as the concentration of \widetilde{NO}_x increases, which raises the risk associated with exposure to
 414 ozone (U.S. EPA, 2020).



415
 416 *Figure 8 : Sensitivity of NO_2 , NO and O_3 concentration to the increase in the \widetilde{NO}_x concentration according to Eq. (21). Zero*
 417 *background concentrations (dashed lines) and background concentrations of the case study ($NO_2 = 34.26 \mu g/m^3$, $NO =$*
 418 *$17.09 \mu g/m^3$, $O_3 = 27.31 \mu g/m^3$, solid lines).*

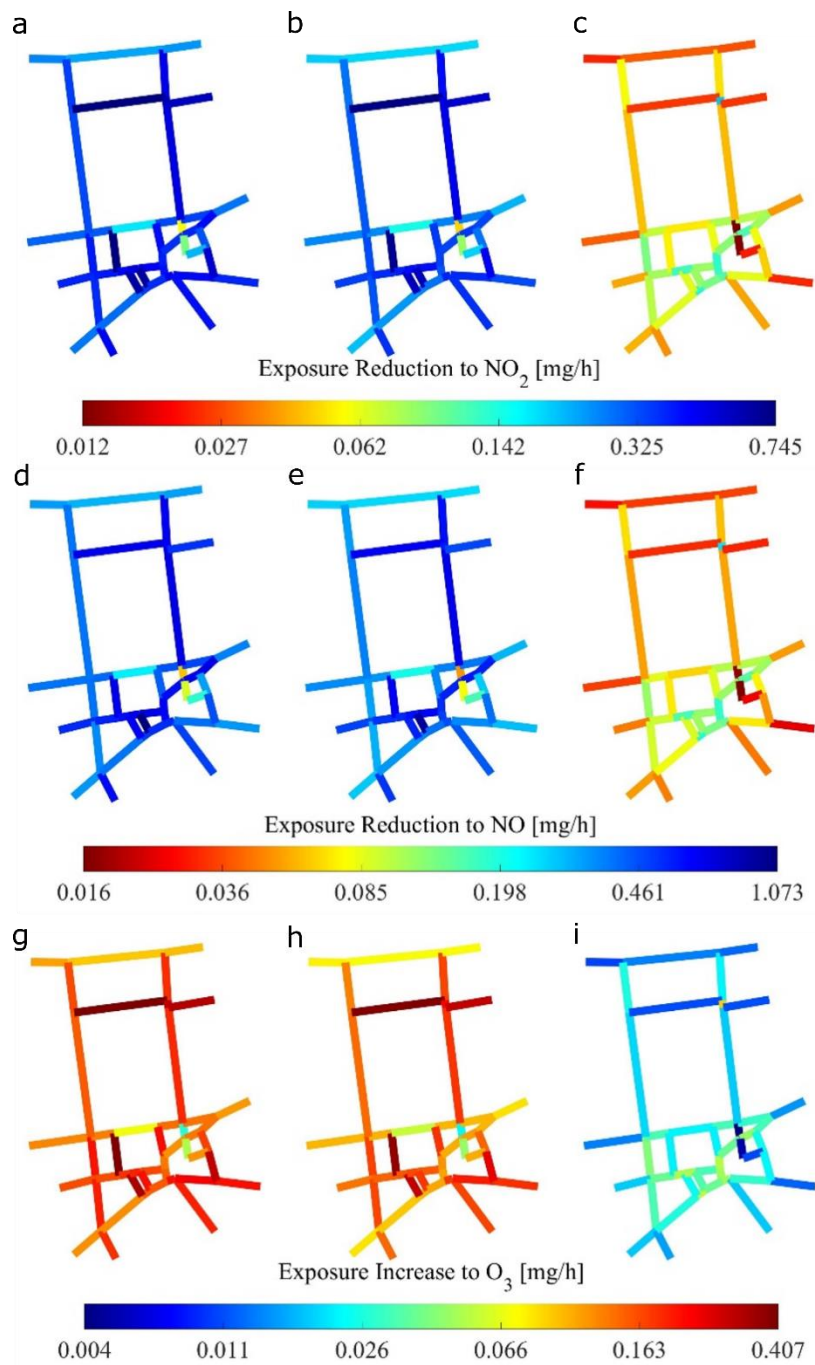
419 5.2 Where to reduce emissions?

420 By substituting the emission sensitivity (26) into Eq. (25), it is straightforward to construct the emission
 421 matrix E for the scenario with photochemical smog and therefore the exposure reduction R by means
 422 of Eq. (12). Below, R is used to identify the best places to reduce emissions in the urban network. As
 423 in section 4.4, an emissions variation $\delta Q = 0.10 \bar{Q}$ is considered for both NO and NO_2 emissions (as
 424 the emissions ratio a is constant).

425

426

427



428

429 *Figure 9: Exposure reduction achieved by decreasing the emission in the street by a constant quantity δQ for NO_2 (a-c) and*
430 *NO (d-f). For O_3 the increase in exposure is shown in (g-i). (a,d,g) and (b,e,h) show the maximum and average values for the*
431 *different wind directions. (c,f,i) show the average computed by neglecting self-interactions. Note the colorbar employs a*
432 *logarithmic scaling.*

433

434 Figure 9 shows the exposure reduction or increase for NO_2 , NO , and O_3 , in the South Kensington case
435 study. As expected, a reduction δQ in NO_x emissions leads to an exposure reduction to nitrogen
436 oxides (Panels a-f). The results are very similar to the passive scalar case (Figure 5), and can nearly be

437 reproduced using a single scaling factor per species. This is due to two reasons: (i) the relation between
438 NO_2 and $\widetilde{\text{NO}}_2$ in the photostationary model is almost linear, especially for large $\widetilde{\text{NO}}_2$ concentration
439 (see Figure 8); and (ii) the background concentration and the ratio α are kept constant for all the
440 streets. Consequently $d\mathbf{g}/d\widetilde{\text{NO}}_x$ has almost constant entries and the matrix E in Eq. (25) is simply
441 rescaled with respect to the case of the passive scalar.

442 On the other hand, panels g-i in Figure 9 evidence an exposure increase to ozone. This is in line with
443 Figure 8 which shows a negative $d\mathbf{g}/d\widetilde{\text{NO}}_x$ for ozone in the case study (solid lines). As explained
444 above, this negative rate depends on the relation between the background and equilibrium ozone
445 concentration. This result highlights that a side effect of the reduction of vehicular traffic may be an
446 increase in ozone concentrations, depending on the background concentrations present in the area.

447 Finally, Figure 8 we remark that the sensitivity analysis presented in this section is dependent on the
448 case study not only due to the dependence of $d\mathbf{g}/d\widetilde{\text{NO}}_x$ on the background concentration but also
449 for its dependence on the initial emissions in the streets which provide $\widetilde{\text{NO}}_x$ concentration (see Eqs.
450 (14)-(15)).

451 **Conclusions**

452 In this work a complex network approach was used to address what is the optimal place to reduce
453 emissions in an urban neighbourhood. Rather than developing a new air quality model, we introduced
454 a mathematical formalism inspired by the theory of complex networks and based on the analysis of
455 physical mechanisms, capable of extending the potential of existing operational tools. In fact, thanks
456 to our approach, it is ultimately possible to reconstruct a large multiplicity of scenarios starting from
457 a single dispersion simulation of a passive scalar.

458 The network was defined by modelling the correlation between emissions and concentrations in
459 streets as weighted links connecting the streets, i.e. the nodes of the network. In this way, the entire
460 process of pollutant dispersion was enclosed in the weight matrix A of the network. By means of this
461 formulation the hypothesis of linearity between emissions and concentrations in the case of non-
462 reactive pollutants was first tested. Then, considering the physics underlying the process, we proposed
463 a linear scaling of matrix A with the intensity of the external wind. In this way, scenarios with different
464 emissions in the streets and different intensity of the external wind could be reproduced using a single
465 weight matrix A_0 constructed from a single dispersion simulation. The network model highlighted the
466 diagonal-dominancy of the problem and suggested a criterion to significantly reduce the
467 computational complexity of the solution, eliminating the less significant network connections.

468 The network description facilitated straightforward translation from polluting concentrations to
469 citizen exposure: a new weight matrix, the exposure matrix, was derived starting from A which took
470 into account the number of people exposed in each street. The outdegree of this new matrix provided
471 a direct metric for exposure reduction in terms of which streets bring the greatest benefits in terms
472 of health impact at the neighbourhood scale.

473 Finally, the model was extended to the analysis of photochemical smog. We used a two-step algorithm
474 to reconstruct the concentrations of reactive pollutants in the streets by applying matrix A and a non-
475 linear function for chemical transformations in the streets. Through a linearization of the exposure
476 model, we obtained an expression of the exposure reduction metric for reacting chemical species and
477 we showed that it can be approximated with a rescaling of the metric for the passive case.

478 The exposure model used in combination with the diagonal dominance of A gave clear indication of
479 what generally the most effective strategy is in terms of health: to reduce emissions in domestic

480 streets with the high aspect ratio H/W , e.g. by making the street one-way. Indeed, the exposure
481 estimate in Eq. (13) is an accurate measure that can be used to estimate total exposure in a street in
482 an operational sense without even the need for a network model.

483 The work presented in this manuscript is straightforward to extend to much larger urban areas, and it
484 is recommended study more realistic emission reduction scenarios, e.g. considering emissions
485 reductions in multiple streets rather than a single street. Further research in the application of metrics
486 and techniques from the theory of complex networks can bring new insights into the analysis of the
487 results and guide administrations in traffic and emission management.

488 Acknowledgements

489 The authors would like to thank Prof. Lionel Soulhac for providing a custom version of SIRANE suitable
490 for source apportionment and for insightful conversations about data assimilation.

491

492 Bibliography

493

494 Anenberg, S. C., Moheggh, A., Goldberg, D. L., Kerr, G. H., Brauer, M., Burkart, K., Hystad, P., Larkin,
495 A., Wozniak, S., & Lamsal, L. (2022). Long-term trends in urban NO₂ concentrations and
496 associated paediatric asthma incidence: estimates from global datasets. *The Lancet Planetary
497 Health*, 6(1), e49–e58. [https://doi.org/10.1016/S2542-5196\(21\)00255-2](https://doi.org/10.1016/S2542-5196(21)00255-2)

498 Baker, J., Walker, H. L., & Cai, X. (2004). A study of the dispersion and transport of reactive pollutants
499 in and above street canyons—a large eddy simulation. *Atmospheric Environment*, 38(39), 6883–
500 6892.

501 Barthelemy, M. (2016). *The structure and dynamics of cities*. Cambridge University Press.

502 Batty, M. (2013). *The new science of cities*. MIT press.

503 Berkowicz, R. (2000). OSPM-A parameterised street pollution model. *Environmental Monitoring and
504 Assessment*, 65(1–2), 323–331.

505 Bloomberg, L., & Dale, J. (2000). Comparison of VISSIM and CORSIM Traffic Simulation Models on a
506 Congested Network. *Transportation Research Record: Journal of the Transportation Research
507 Board*, 1727(1), 52–60. <https://doi.org/10.3141/1727-07>

508 Boccaletti, S., Latora, V., Moreno, Y., Chavez, M., & Hwang, D.-U. (2006). Complex networks:
509 Structure and dynamics. *Physics Reports*, 424(4–5), 175–308.

510 Bright, V. B., Bloss, W. J., & Cai, X. (2013). Urban street canyons: Coupling dynamics, chemistry and
511 within-canyon chemical processing of emissions. *Atmospheric Environment*, 68, 127–142.

512 Carpentieri, M., Salizzoni, P., Robins, A., & Soulhac, L. (2012). Evaluation of a neighbourhood scale,
513 street network dispersion model through comparison with wind tunnel data. *Environmental
514 Modelling and Software*, 37, 110–124. <https://doi.org/10.1016/j.envsoft.2012.03.009>

515 Clappier, A., Belis, C. A., Pernigotti, D., & Thunis, P. (2017). Source apportionment and sensitivity
516 analysis: two methodologies with two different purposes. *Geoscientific Model Development*,
517 10(11), 4245–4256. <https://doi.org/10.5194/gmd-10-4245-2017>

- 518 Derwent, R. G., & Middleton, D. R. (1996). An empirical function for the ratio NO sub (2): NO sub (x).
519 *Clean Air*, 26(3), 57–60.
- 520 EEA. (2022). *Managing air quality in Europe*.
- 521 Epa, U., & Factors Program, E. (2011). *Exposure Factors Handbook: 2011 Edition*. www.epa.gov
- 522 Fellini, S., Salizzoni, P., & Ridolfi, L. (2020). Centrality metric for the vulnerability of urban networks
523 to toxic releases. *Physical Review E*, 101(3), 32312.
- 524 Fellini, S., Salizzoni, P., & Ridolfi, L. (2021). Vulnerability of cities to toxic airborne releases is written
525 in their topology. *Scientific Reports*, 11(1). <https://doi.org/10.1038/s41598-021-02403-y>
- 526 Fellini, S., Salizzoni, P., Soulhac, L., & Ridolfi, L. (2019). Propagation of toxic substances in the urban
527 atmosphere: A complex network perspective. *Atmospheric Environment*, 198, 291–301.
- 528 Greater London Authority. (n.d.). *London Average Air Quality Levels - London Datastore*. Retrieved
529 April 1, 2022, from <https://data.london.gov.uk/dataset/london-average-air-quality-levels>
- 530 Grewe, V., Tsati, E., & Hoor, P. (2010). On the attribution of contributions of atmospheric trace gases
531 to emissions in atmospheric model applications. *Geoscientific Model Development*, 3(2), 487–
532 499. <https://doi.org/10.5194/gmd-3-487-2010>
- 533 Grylls, T., le Cornec, C. M. A., Salizzoni, P., Soulhac, L., Stettler, M. E. J., & van Reeuwijk, M. (2019).
534 Evaluation of an operational air quality model using large-eddy simulation. *Atmospheric*
535 *Environment: X*, 3, 100041. <https://doi.org/10.1016/J.AEAOA.2019.100041>
- 536 Iacobello, G., Marro, M., Ridolfi, L., Salizzoni, P., & Scarsoglio, S. (2019). Experimental investigation of
537 vertical turbulent transport of a passive scalar in a boundary layer: Statistics and visibility graph
538 analysis. *Physical Review Fluids*, 4(10), 104501.
- 539 Int Panis, L., Broekx, S., & Liu, R. (2006). Modelling instantaneous traffic emission and the influence
540 of traffic speed limits. *Science of The Total Environment*, 371(1–3), 270–285.
541 <https://doi.org/10.1016/j.scitotenv.2006.08.017>
- 542 Kakosimos, K. E., Hertel, O., Ketzler, M., & Berkowicz, R. (2010). Operational Street Pollution Model
543 (OSPM) - a review of performed application and validation studies, and future prospects.
544 *Environmental Chemistry*, 7(6), 485. <https://doi.org/10.1071/EN10070>
- 545 Khreis, H., Kelly, C., Tate, J., Parslow, R., Lucas, K., & Nieuwenhuijsen, M. (2017). Exposure to traffic-
546 related air pollution and risk of development of childhood asthma: A systematic review and
547 meta-analysis. In *Environment International* (Vol. 100, pp. 1–31). Elsevier Ltd.
548 <https://doi.org/10.1016/j.envint.2016.11.012>
- 549 Kim, Y., Wu, Y., Seigneur, C., & Roustan, Y. (2018). Multi-scale modeling of urban air pollution:
550 development and application of a Street-in-Grid model (v1. 0) by coupling MUNICH (v1. 0) and
551 Polair3D (v1. 8.1). *Geoscientific Model Development*, 11(2), 611–629.
- 552 Koo, B., Wilson, G. M., Morris, R. E., Dunker, A. M., & Yarwood, G. (2009). Comparison of Source
553 Apportionment and Sensitivity Analysis in a Particulate Matter Air Quality Model.
554 *Environmental Science & Technology*, 43(17), 6669–6675. <https://doi.org/10.1021/es9008129>
- 555 Lu, J., Li, B., Li, H., & Al-Barakani, A. (2021). Expansion of city scale, traffic modes, traffic congestion,
556 and air pollution. *Cities*, 108, 102974. <https://doi.org/10.1016/j.cities.2020.102974>

- 557 McHugh, C. A., Carruthers, D. J., & Edmunds, H. A. (1997). ADMS-Urban: an air quality management
558 system for traffic, domestic and industrial pollution. In *Int. J. Environment and Pollution* (Vol. 8).
- 559 McHugh, C. A., Carruthers, D. J., & Edmunds, H. A. (1997). ADMS–Urban: an air quality management
560 system for traffic, domestic and industrial pollution. *International Journal of Environment and*
561 *Pollution*, 8(3–6), 666–674.
- 562 Newman, M. (2010). *Networks*. Oxford University Press.
563 <https://doi.org/10.1093/acprof:oso/9780199206650.001.0001>
- 564 Oke, T. R., Mills, G., Christen, A., & Voogt, J. A. (2017). *Urban Climates*. Cambridge University Press.
565 <https://doi.org/10.1017/9781139016476>
- 566 Park, N. (2020). Population-estimates-for-the-UK-England-and-Wales-Scotland-and-Northern-
567 Ireland-provisional-mid-2019. *Hampshire: Office for National Statistics*.
- 568 Salizzoni, P., Soulhac, L., & Mejean, P. (2009). Street canyon ventilation and atmospheric turbulence.
569 *Atmospheric Environment*, 43(32), 5056–5067.
570 <https://doi.org/10.1016/j.atmosenv.2009.06.045>
- 571 Ser-Giacomi, E., Baudena, A., Rossi, V., Vasile, R., Lopez, C., & Hernández-Garca, E. (2019). From
572 network theory to dynamical systems and back: Lagrangian Betweenness reveals bottlenecks in
573 geophysical flows. *ArXiv Preprint ArXiv:1910.04722*.
- 574 Soulhac, L., Nguyen, C. v., Volta, P., & Salizzoni, P. (2017). The model SIRANE for atmospheric urban
575 pollutant dispersion. PART III: Validation against NO₂ yearly concentration measurements in a
576 large urban agglomeration. *Atmospheric Environment*, 167, 377–388.
577 <https://doi.org/10.1016/j.atmosenv.2017.08.034>
- 578 Soulhac, L., Puel, C., Duclaux, O., & Perkins, R. J. (2003). Simulations of atmospheric pollution in
579 Greater Lyon an example of the use of nested models. *Atmospheric Environment*, 37(37), 5147–
580 5156. <https://doi.org/10.1016/j.atmosenv.2003.03.002>
- 581 Soulhac, L., & Salizzoni, P. (2010). Dispersion in a street canyon for a wind direction parallel to the
582 street axis. *Journal of Wind Engineering and Industrial Aerodynamics*, 98(12), 903–910.
583 <https://doi.org/10.1016/j.jweia.2010.09.004>
- 584 Soulhac, L., Salizzoni, P., Cierco, F. X., & Perkins, R. (2011a). The model SIRANE for atmospheric urban
585 pollutant dispersion; part I, presentation of the model. *Atmospheric Environment*, 45(39),
586 7379–7395.
- 587 Soulhac, L., Salizzoni, P., Cierco, F. X., & Perkins, R. (2011b). The model SIRANE for atmospheric
588 urban pollutant dispersion; part I, presentation of the model. *Atmospheric Environment*,
589 45(39), 7379–7395. <https://doi.org/10.1016/j.atmosenv.2011.07.008>
- 590 Soulhac, L., Salizzoni, P., Cierco, F.-X., & Perkins, R. (2011c). The model SIRANE for atmospheric
591 urban pollutant dispersion; part I, presentation of the model. *Atmospheric Environment*,
592 45(39), 7379–7395.
- 593 Soulhac, L., Salizzoni, P., Mejean, P., Didier, D., & Rios, I. (2012). The model SIRANE for atmospheric
594 urban pollutant dispersion; PART II, validation of the model on a real case study. *Atmospheric*
595 *Environment*, 49, 320–337. <https://doi.org/10.1016/j.atmosenv.2011.11.031>

596 UK Ambient Air Quality Interactive Map. (n.d.). Retrieved April 1, 2022, from [https://uk-](https://uk-air.defra.gov.uk/data/gis-mapping/)
597 [air.defra.gov.uk/data/gis-mapping/](https://uk-air.defra.gov.uk/data/gis-mapping/)

598 U.S. EPA. (2020). *Integrated Science Assessment (ISA) for Ozone and Related Photochemical Oxidants*
599 *(Final Report, Apr 2020)*.

600 Wagstrom, K. M., Pandis, S. N., Yarwood, G., Wilson, G. M., & Morris, R. E. (2008). Development and
601 application of a computationally efficient particulate matter apportionment algorithm in a
602 three-dimensional chemical transport model. *Atmospheric Environment*, *42*(22), 5650–5659.
603 <https://doi.org/10.1016/J.ATMOSENV.2008.03.012>

604 Wang, Z. S., Chien, C.-J., & Tonnesen, G. S. (2009). Development of a tagged species source
605 apportionment algorithm to characterize three-dimensional transport and transformation of
606 precursors and secondary pollutants. *Journal of Geophysical Research*, *114*(D21).
607 <https://doi.org/10.1029/2008jd010846>

608 WHO. (2021). *WHO global air quality guidelines: particulate matter (PM_{2.5} and PM₁₀), ozone,*
609 *nitrogen dioxide, sulfur dioxide and carbon monoxide*.

610 Wu, Y., Zhang, S., Hao, J., Liu, H., Wu, X., Hu, J., Walsh, M. P., Wallington, T. J., Zhang, K. M., &
611 Stevanovic, S. (2017). On-road vehicle emissions and their control in China: A review and
612 outlook. *Science of The Total Environment*, *574*, 332–349.
613 <https://doi.org/10.1016/J.SCITOTENV.2016.09.040>

614 Zhang, K., Chen, G., Zhang, Y., Liu, S., Wang, X., Wang, B., & Hang, J. (2020). Integrated impacts of
615 turbulent mixing and NO_x-O₃ photochemistry on reactive pollutant dispersion and intake
616 fraction in shallow and deep street canyons. *Science of the Total Environment*, *712*, 135553.

617